

# Cell-Free Layer (CFL) Measurements in Complex Geometries: Contractions and Bifurcations

Susana Novais, Diana Pinho, David Bento, Elmano Pinto, Tomoko Yaginuma, Carla S. Fernandes, Valdemar Garcia, Ana I. Pereira, José Lima, Maite Mujika, Ricardo Dias, Sergio Arana and Rui Lima

**Abstract** In this chapter we discuss the cell-free layer (CFL) developed adjacent to the wall of microgeometries containing complex features representative of the microcirculation, such as contractions, expansions, bifurcations and confluences. The microchannels with the different geometries were made of polydimethylsiloxane (PDMS) and we use optical techniques to evaluate the cell-free layer for red blood cells (RBCs) suspensions with different hematocrit (Hct). The

---

S. Novais (✉) · D. Pinho · D. Bento · E. Pinto · T. Yaginuma · C. S. Fernandes · V. Garcia · A. I. Pereira · J. Lima · R. Dias · R. Lima  
Polytechnic Institute of Bragança, ESTiG/IPB, C. Sta. Apolónia 5301-857 Bragança, Portugal  
e-mail: sc2005@sapo.pt

D. Pinho  
e-mail: diana@ipb.pt

D. Bento  
e-mail: davidbento@ipb.pt

E. Pinto  
e-mail: elmanopinto@ipb.pt

T. Yaginuma  
e-mail: tyaginuma09@gmail.com

C. S. Fernandes  
e-mail: cveiga@ipb.pt

V. Garcia  
e-mail: Valdemar@ipb.pt

A. I. Pereira  
e-mail: apereira@ipb.pt

J. Lima  
e-mail: jllima@ipb.pt

R. Dias  
e-mail: ricardod@ipb.pt

images are captured using a high-speed video microscopy system and the thickness of the cell-free layer was measured using both manual and automatic image analysis techniques. The results show that in *in vitro* microcirculation, the hematocrit and the geometrical configuration have a major impact on the CFL thickness. In particular, the thickness of the cell-free layer increases as the fluid flows through a contraction–expansion sequence and that this increase is enhanced for lower hematocrit. In contrast, the flow rates tested in these studies did not show a clear influence on the CFL thickness.

## 1 Introduction

Human blood is a complex fluid composed mainly of suspended deformable red blood cells (RBCs) within plasma. The RBCs are responsible for the supply of oxygen and nutrients to the body and removal of carbon dioxide and metabolic wastes from tissues. Blood flow behaviour in microcirculation depends on several combined effects such as cell deformability, flow shear rates and geometry of the microvessel, as well as biochemical and biophysical factors which may also affect the rheological characteristics of blood.

A well known hemodynamic phenomenon, known as Fahraeus-Lindqvist effect, observed in both *in vivo* and *in vitro* studies states that for narrow microtubes ( $<300\ \mu\text{m}$ ) both hematocrit and apparent blood viscosity decreases as the tube diameter is reduced (Pires et al. 1992, Goldsmith et al. 1989). The physical reason behind this phenomenon is related to the tendency of the RBCs to undergo axial migration induced by the tank treading motion of its deformable cell membrane as a result of the high shear stresses developed around the wall, and the parabolic velocity profile which forces the RBCs to move towards the center of the vessel (Caro et al. 1978, Garcia et al. 2012, Maeda 1996a, Lima et al. 2012a),

---

R. Lima  
e-mail: ruimec@ipb.pt

D. Pinho · D. Bento · E. Pinto · R. Dias · R. Lima  
CEFT, Faculdade de Engenharia da Universidade do Porto (FEUP), 4200-465 Porto,  
Portugal

A. I. Pereira  
Algoritmi University of Minho, Braga, Portugal

J. Lima  
INESC, Faculdade de Engenharia da Universidade do Porto (FEUP), Porto, Portugal

M. Mujika · S. Arana  
CEIT and Tecnun, University of Navarra, Paseo de Manuel Lardizábal No 15 20.018  
Donostia-San Sebastián, Spain  
e-mail: mmujika@ceit.es

S. Arana  
e-mail: sarana@ceit.es

consequently leading to the formation of two phases, i. e., a flow core with mainly RBCs and a cell-free layer (CFL) (Lima et al. 2009a, Fujiwara et al. 2009, Lima et al. 2009b). The CFL formation in microvessels reduces the apparent viscosity of blood and by increasing the CFL thickness the blood viscosity decreases in both microchannels and microvessels. Hence, it is extremely important to understand the behavior of the CFL in microcirculation as it contributes to the rheological properties of blood flowing in microvessels, it modulates the nitric oxide scavenging effects by RBCs and it may lead to heterogeneous distribution of blood cells in microvascular networks (Fedosov et al. 2010, Kim et al. 2009).

The cell-free layer width or thickness can be defined as the distance between the wall of the microchannel and the boundary region of the RBCs core. Although the formation of the CFL *in vivo* (Maeda et al. 1996b, Tateishi et al. 1994) has been of great interest over many years, little information is available about this phenomena due to the limitations of the measurement techniques and the complexity of the vascular network. Various researchers have attempted to replicate this behaviour *in vitro* using microfluidic systems in order to better understand this phenomena and explore its potential as a new diagnostic tool (Fujiwara et al. 2009, Lima et al. 2009b). Shevkoplyas et al. (2005) developed a microdevice to isolate WBCs from a blood sample by using the margination effect, whereas Hou et al. (2010) have proposed, very recently, a biomimetic separation device to separate normal and malaria infected RBCs. Other researchers have found several advantages to control and manipulate blood flow in microfluidic devices. Fujiwara et al. (2009) have found evidence that not only it is possible to create an artificial CFL under appropriate hemodynamic and geometrical conditions but also the CFL thickness is strongly influenced by the RBC deformability.

According to Kim et al. (2009) the width of the CFL generally decreases with increasing hematocrit (Hct). The physiological conditions of the working fluid have also a significant influence on the CFL (Maeda 1996, Lima et al. 2012a), and the geometry of the microchannel is another factor that influences the CFL thickness (Sollier et al. 2010, Faivre et al. 2006).

Manual tracking methods have been used extensively to study the blood flow behaviour in microchannels. Examples are the tracking of individual RBCs flowing through glass capillaries (Lima et al. 2007, 2008, 2009a, 2012b, Suzuki et al. 1996), straight polydimethylsiloxane (PDMS) microchannels with rectangular cross-section (Fujiwara et al. 2009), stenosis (Lima et al. 2009a), hyperbolic contractions (Yaginuma et al. 2011, 2013) and bifurcations (Leble et al. 2011, Lima et al. 2011). Manual methods can be highly reliable but they are relatively time consuming and are more subject to user errors. As a result, it is essential to develop image analysis methods able to process the data automatically. Some researchers have already proposed automatic methods to obtain automatically the trajectories of labelled RBCs (Pinho et al. 2012, 2013) or to measure the CFL thickness in microvessels (Kim et al. 2006, Namgung et al. 2010).

In this paper we present an automatic method based in a sequence of simple steps such as the noise reduction by applying pre-processing filters and images binarization by applying threshold levels (Eddins et al. 2002, Bovik 2009). The

main purpose is to examine the effect of different artificial contractions, bifurcations and confluences, different hematocrits (Hct) and different velocities in the CFL thickness. In this study, we expect to improve our understanding about the effect of both geometries and Hct on the CFL thickness and that will be crucial to optimize the design of a microfluidic device able to perform in a single step blood separation and cell deformability measurements.

The current chapter is divided in two main parts: in the first part we use a manual tracking plugin from Image J (Abramoff et al. 2004) to study the effect of sudden contraction followed by a sudden expansion on the CFL thickness whereas in the second part we discuss an automatic method for image analysis using MatLab (2010), to obtain the CFL thickness along a microchannel containing several diverging and converging bifurcations.

## 2 Materials and Methods

### 2.1 Microchannels Fabrication and Geometry

The microchannels fabricated for the proposed assays have been produced in PDMS by softlithography from a photo-resist mold. An overview of the fabrication procedure is illustrated in Fig. 1. First, the mold was fabricated by photolithographic technique on a silicon (Si) wafer with an ultra-thick photoresist (SU-8). In this process, a layer of SU-8 photoresist was spin-coated onto the Si wafer and patterned by UV exposure through a photomask. After various curing steps, a SU-8 developer was then used to obtain the final mold master containing the inverse of the desired microchannels.

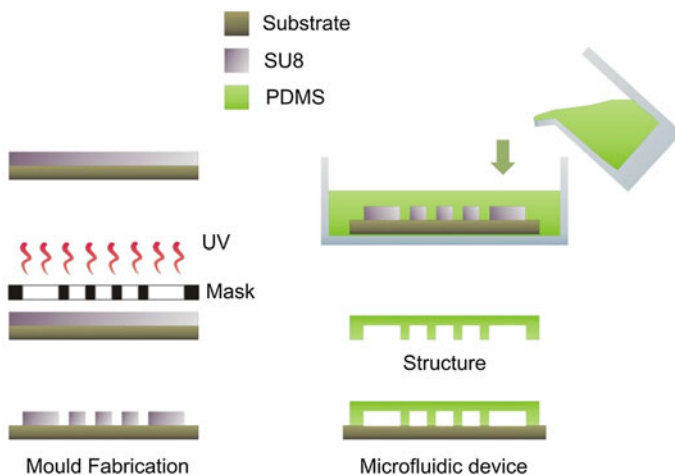


**Fig. 1** Main steps of the PDMS microfluidic devices fabrication procedure

The PDMS was prepared by mixing a base and curing agent at a weight ratio of 10:1 for the channels, and 20:1 for the glass slide. After removing the bubbles created during the mixing steps, the mixture was poured over the mold master and baked in the oven for about 20 min at 80 °C. The PDMS is then removed from the mold, cooled to room temperature and the input/output ports were made with an appropriate punching.

Finally, the three-dimensional PDMS microchannel structure was sealed with a glass slide previously spin-coated with PDMS and baked in the oven for 20 min at 80 °C. After this procedure the microfluidic device returns to the oven for further 24 h for a strong seal.

For the first study, the geometry used was a straight channel 400 μm wide containing a sudden contraction 20 μm in width followed by a sudden expansion (see Fig. 2a). The expansion ratio of the geometries,  $r_e$ , is given by:

$$r_e = \frac{w_1}{w_2} \tag{1}$$

where  $w_1$  is the dimension of the large channel and  $w_2$  is the dimension of the narrow channel (see Fig. 2) in the contraction region.

In the second study the geometry used is more complex, containing several bifurcations and confluences (see Fig. 2b). Figure 2 illustrate the configuration and relevant dimensions of the geometries used in both studies.

### 2.2 Experimental Set-up and Working Fluids

The blood samples used were collected from a healthy adult sheep, and ethylenediaminetetraacetic acid (EDTA) was added to prevent coagulation. The RBCs were separated from the blood by centrifugation and washed twice with physiological saline (PS). The washed RBCs were suspended in Dextran 40 (Dx 40) to make up the required RBCs concentration by volume. All blood samples were

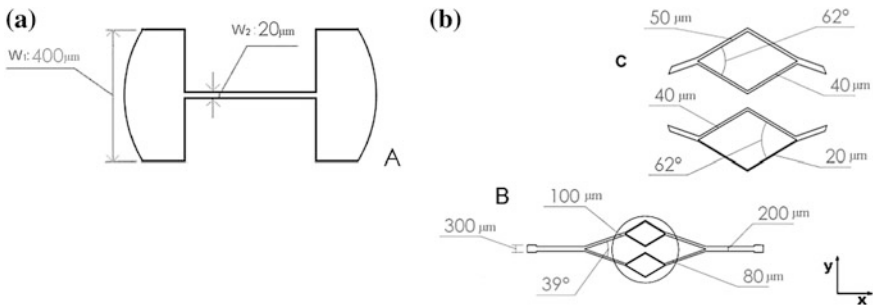
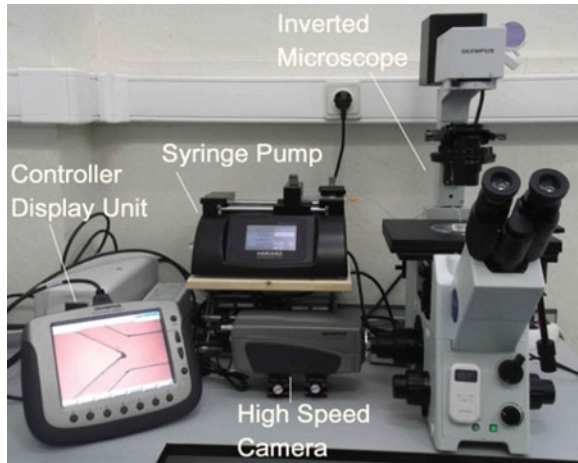


**Fig. 2** Geometry and dimensions of the microchannels; **a** contraction–expansion geometry used in the first study, A (scale 50:1); **b** bifurcation–confluence geometry used for the second study, B (scale 6:1) and a detail view C (scale 15:1)

**Fig. 3** Micro-PTV experimental set-up



stored hermetically at 4 °C until the experiment was performed at an ambient temperature of about 22 °C.

The micro-particle tracking velocimetry (PTV) system used in the present study consists of an inverted microscope (IX71, Olympus) combined with a high-speed camera (*i*-SPEED LT, Olympus) (see Fig. 3). The PDMS microchannel was placed on the stage of the microscope where the flow rate of the working fluids was kept constant by means of a syringe pump (PHD ULTRA) with a 5 ml syringe (TERUMO<sup>®</sup> SYRING).

The series of  $x$ - $y$  images were captured with a resolution of  $600 \times 800$  pixels. All images were recorded at the center plane of the microchannels at a rate of 600 frames/sec for the first experiment and of 200 frames/sec for the second experiment and were transferred to the computer and then evaluated using image analysis.

## 2.3 Image Analysis

### 2.3.1 Manual Method

MTrackJ plugin (Meijering et al. 2006), available for ImageJ was used to automatically computed the centroid of the selected RBC. After obtaining  $x$  and  $y$  positions, the data were exported for the determination of each individual RBC trajectory, Fig. 4.

This method was used in both studies to obtain the data. In the first study the manual data was used to measure the CFL thickness and in the second study the manual data was used for comparison with the measurements obtained by the proposed automatic method.

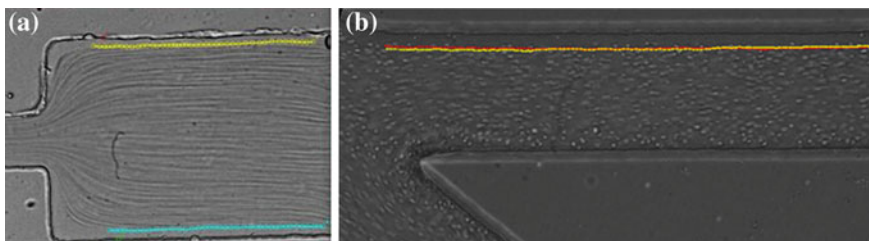


**Fig. 4** Manual method showing the trajectories of labeled RBC: **a** for an expansion geometry; **b** for a bifurcation geometry

### 2.3.2 Automatic Method

All image sequences were processed using Image Processing toolbox available in MatLab (Abramoff et al. 2004) and an automatic method is developed and tested, Automatic Method.

Firstly a median filter with a  $3 \times 3$  pixel mask was applied to each frame to reduce the noise of the images. Then, the intensity of each pixel in the frame sequence was evaluated to obtain an image with the maximum intensity, with this step is possible identified the region of biggest concentration of blood cells and the region where blood cells don't exist, the plasma layer. As a final step, the image was converted into a binary image, (Fig. 5b). Finally, the region of interest is selected and the upper CFL trajectories are automatically measured. Figure 5 shows the image processing result for the developed method.

### 2.3.3 Procedures to Measure the CFL Thickness

To analyze the CFL thickness, measurements were taken upstream (before) and downstream (after) the artificial contraction region, as show in Fig. 6:  $CFL_u$  corresponds to the thickness of the CFL upstream the contraction, and the  $CFL_d$  to the thickness downstream the contraction. The difference of the CFL upstream and downstream of the contraction is given by:

$$\Delta_{CFL} = CFL_d - CFL_u \quad (2)$$

A positive difference indicates an expansion of the CFL.

## 3 Results and Discussion

In this section the data obtained from both studies is analysed and discussed.

**Fig. 5** Results from the automatic method: **a** Original image; **b** Binary image obtained by Automatic Method

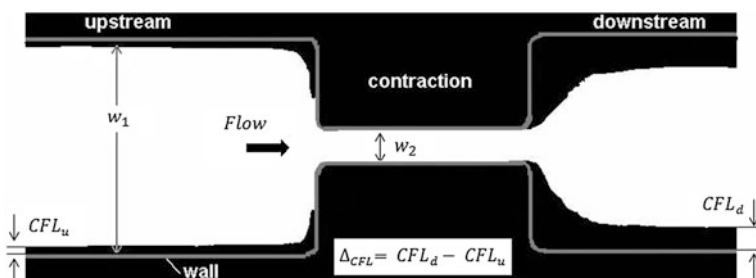
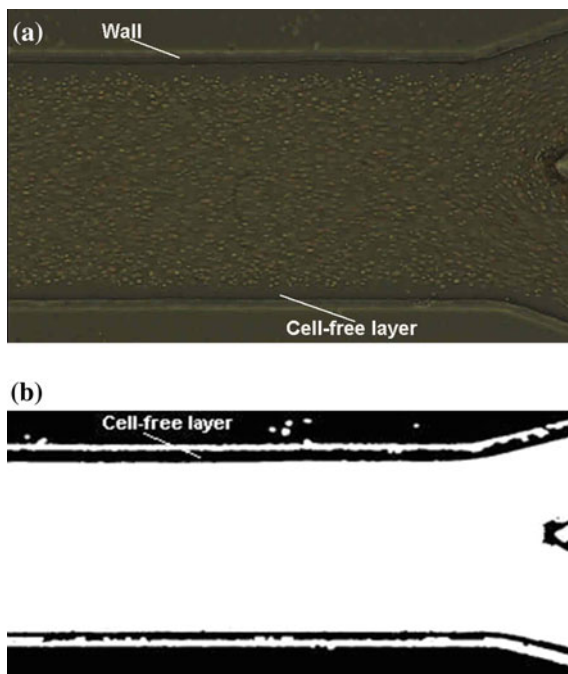


**Fig. 6** Schematic view of the contraction–expansion geometry, identifying the relevant variables

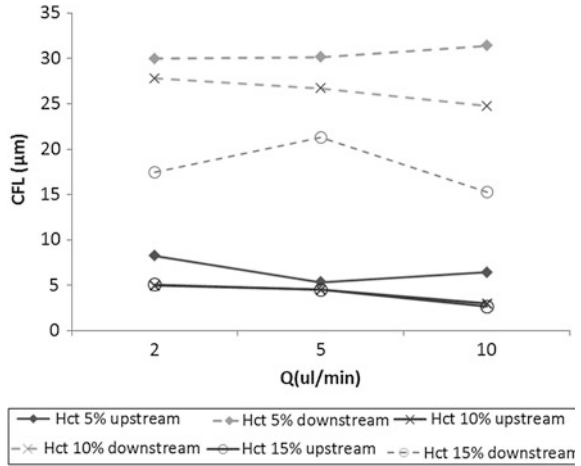
In the first study, the geometry used is presented in (Fig. 3a). This geometry has an expansion ratio of 20 and experiments with three distinct hematocrits, 5, 10 and 15 %, and three different flow rates, 2, 5 and 10  $\mu\text{l}/\text{min}$  have been performed.

The results of the CFL represented in the diagrams below show the effect of hematocrit at different flow rates, and the effect of contraction on the CFL thickness. To analyse the influence of the contraction on CFL thickness the CFL difference between upstream ( $CFL_u$ ) and downstream ( $CFL_d$ ) the contraction was calculated (see Fig. 6).

In Fig. 7, one can analyze the effect of the Hct and flow rate on the thickness of the CFL.



**Fig. 7** CFL thickness upstream and downstream for 5, 10 and 15 % Hct



The results suggest that, for a 5 % of Hct, the cell-free layer has significantly higher values downstream of the contraction. In general terms, nothing can be concluded regarding the influence that flow rate may have on the thickness of the CFL, but comparing the CFL before and after the contraction, the results suggest that the CFL is about 4.6 times bigger after the contraction than before the contraction.

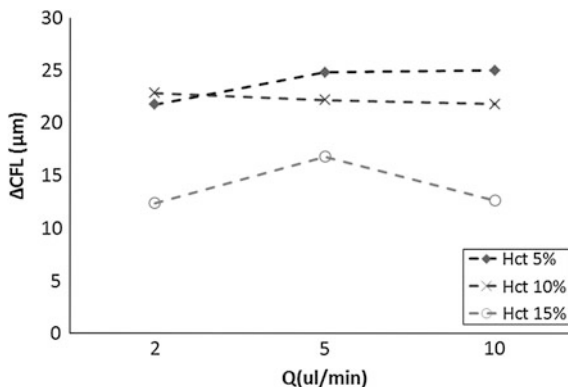
In addition to the considerations made previously, for a 10 % Hct again it is visible the increase in CFL thickness after the contraction, and this sustained an average increase of about 5.9 times. The data from the 15 % Hct, it is concluded again that the CFL, as for 5 and 10 % of hematocrit, is higher than upstream of the contraction, and this contraction downstream of the CFL thickness is about 4.4 times larger than the upstream of contraction.

These results suggest that the contraction provides an increased thickness of the CFL. Moreover, the results of the CFL obtained from downstream of the contraction suggest that increasing the Hct promotes a slight decrease in the CFL.

Figure 8 shows an analysis for all Hcts in relation to the CFL difference,  $\Delta_{CFL}$ , of the CFL upstream and downstream of the contraction as a function of the flow rates 2, 5 and 10  $\mu\text{l}/\text{min}$ . Generally, the results suggest that an increase in Hct involves a reduction in the difference of the CFL. Taking as an example, for the second flow rate (5  $\mu\text{l}/\text{min}$ ), the previous conclusion is strengthened, since it is found that for a 5 % Hct there is a  $\Delta_{CFL}$  of 22.8  $\mu\text{m}$ , then with a Hct 10 % there is a reduction of 7.21  $\mu\text{m}$  for  $\Delta_{CFL}$ . Finally, for the Hct 15 %,  $\Delta_{CFL}$  has the smallest of 12.4  $\mu\text{m}$ , i.e. the increase in Hct implies a reduction in  $\Delta_{CFL}$  and therefore a reduction in the formation of the CFL.

For the second study we have used the geometry presented in the (Fig. 2 b) and the results were taken in the sections represented in the Fig. 9, i.e., sections CFL<sub>A,B,C</sub> represents the results obtained upstream of the middle of the geometry and section CFL<sub>D,E,F</sub> the results obtained downstream of the middle of the

**Fig. 8** CFL difference ( $\Delta_{CFL}$ ) of the contractions for all Hcts as a function of the flow rate of 2, 5 and 10  $\mu\text{l}/\text{min}$



geometry. In this study it was applied the manual method used in the first study and then was applied the automatic method already described in the Sect. 2.

In this study we used two different hematocrits, 5 and 10 % and the same velocity for both, 500  $\text{nl}/\text{min}$ , and the results obtained by the automatic method were compared with manual results obtained by using a manual tracking method (MtrackJ) from Image J.

As we can see in Table 1, the data obtained from the automatic method, in different regions of geometry analysis, present some discrepancy compared with results obtained manually. This discrepancy occurs because, when performing the binarization of the image with the maximum intensity, parts of the walls of the channels are added to CFL, this is because the intensity of the CFL and the walls are very close. To minimize some of the errors in automatic method we can apply different levels of thresholding and obtain data more close to those obtained manually. However, it is possible to observe in the Fig. 10, there is a similar behaviour between the results obtained by automatic method and manual method for both hematocrits. As example in the case of the hematocrit 5 %, the both methods have a different data, separated for more or less 10  $\mu\text{m}$ , though both have the same behaviour along the channel.

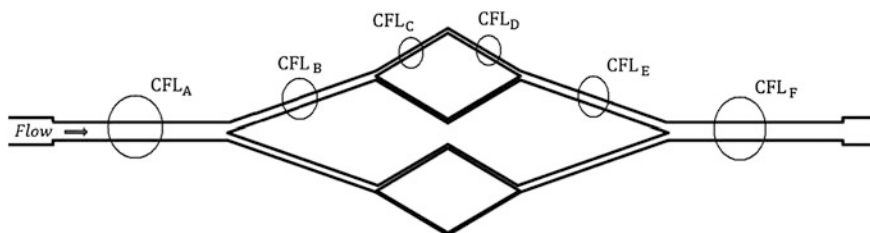


**Fig. 9** Visualization the regions where the data was taken

**Table 1** - Comparison between the manual and automatic data for CFL ( $\mu\text{m}$ )

<i>Hct</i> (%)		<i>CFL<sub>A</sub></i>	<i>CFL<sub>B</sub></i>	<i>CFL<sub>C</sub></i>	<i>CFL<sub>D</sub></i>	<i>CFL<sub>E</sub></i>	<i>CFL<sub>F</sub></i>
5	Manual	15.377	15.564	10.668	10.481	11.755	12.409
	Automatic	22.582	25.431	18.689	17.996	22.487	21.321
10	Manual	9.917	9.184	7.623	8.179	9.448	9.875
	Automatic	12.218	12.694	8.0146	10.867	16.301	15.201

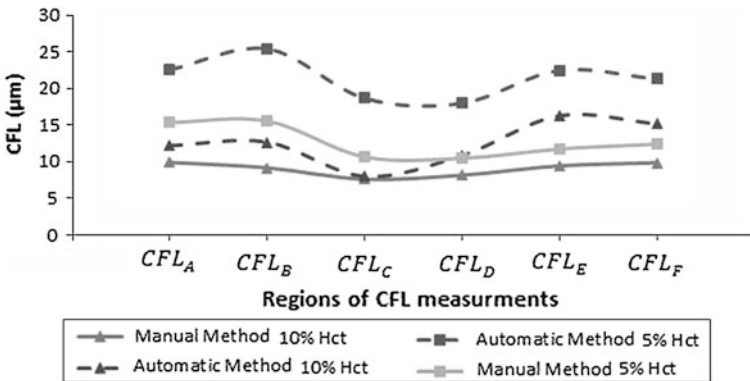


**Fig. 10** Comparison between the data obtained manually and automatically

Other visible influence is a decrease in the CFL when Hct increase, and it is verified a tendency to reduce the CFL comparing the *CFL<sub>A</sub>* with the *CFL<sub>F</sub>* for both hematocrits.

### 4 Conclusions and Future Directions

Regarding the analysis of the variation of CFL thickness, it can be stated that the geometry created with an expansion ratio of 20, led to a series of obstacles, such as clogging of microchannels due to the very small size of the contraction. However, it should be noted that with this geometry, high values been obtained for the CFL, then it can be concluded that the expansion ratio influences the thickness of the CFL. Additionally, the results also demonstrate that the CFL is always higher in the downstream than the upstream of the contraction. When comparing the values of the difference of thickness of the CFL (upstream–downstream), it is evident that the fluid with a 5 % Hct is the one having greater values, followed by the fluid with a Hct of 10 % and finally the fluid with an Hct of 15 %. Note that for the second study, where we used two different methods (one manual and one automatic) the results corroborate the data obtained from the first study, i.e., the CFL decreases as the Hct increases.

Image analysis plays an important role in this kind of studies but the image quality and the conditions of the recorded videos are also important steps for a reliable image processing. Although the proposed automatic method presents satisfactory results, in the near future we plan to improve the quality and resolution of the images and also the processing steps to obtain results closer to the reality. Additionally, for the first study we also plan in the near future to optimize the geometry in order to achieve one biomedical microdevice with the capability of in one single step, to separate the blood cells that exist in the CFL and measure the deformability of these cells. According to some researchers a microdevice with this skill will be interesting for a direct and rapid diagnosis of some diseases since it will allow studies with different blood cells in the presence of some diseases and separate a specific constituent from blood.

**Acknowledgments** The authors acknowledge the financial support provided by: PTDC/SAU-BEB/108728/2008, PTDC/SAU-BEB/105650/2008, PTDC/EME-MFE/099109/2008 and PTDC/SAU-ENB/116929/2010 from FCT (Science and Technology Foundation), COMPETE, QREN and European Union (FEDER). The authors are grateful to Mónica Oliveira for many valuable comments on this study.

## References

- Abramoff M, Magelhaes P, Ram S (2004) Image processing with image. *J Int Biophotonics* 11:36–42
- Bovik A (2009) *The essential guide to image processing*. Elsevier, Burlington
- Caro C, Pedley T, Schroter R, Seed W (1978). *The mechanics of the circulation*. Oxford University Press, USA
- Eddins SL, Gonzalez RC, Woods RE (2002). *Digital image processing using matlab*. Prentice Hall, NJ
- Faivre M, Abkarian M, Bickraj K, Stone H (2006) Geometrical focusing of cells in a microfluidic device: an approach to separate blood plasma. *Biorheology* 43:147
- Fedosov DA, Caswell B, Popel AS, Karniadakis G (2010) Blood flow and cell-free layer in microvessels. *Microcirculation* 17(8):615–628
- Fujiwara H, Ishikawa T, Lima R, Matsuki N, Imai Y, Kaji H, Nishizawa M, Yamaguchi T (2009) Red blood cell motions in high-hematocrit blood flowing through a stenosed microchannel. *J Biomech* 42:838–843
- Garcia V, Dias R, Lima R (2012). In vitro blood flow behaviour in microchannels with simple and complex geometries. In: Dr. Ganesh R.N (ed) *Applied biological engineering—principles and practice*, ISBN: 978-953-51-0412-4. InTech, 393–416
- Goldsmith H, Cokelet G, Gahtgens P (1989) Robin Fahraeus: evolution of his concepts in cardiovascular physiology. *Am J Physiol* 257:H1005–H10015
- Hou HW, Bhagat AA, Chong AG, Mao P, Tan KS, Han J, Lim CT (2010) Deformability based cell margination—a simple microfluidic design for malaria-infected erythrocyte separation. *Lab Chip* 10:2605–2613
- Kim S, Kong RL, Popel AS, Intaglietta M, Johnson PC (2006) A computer—based for determination of cell-free layer width in microcirculation. *Microcirculation* 13:199–207
- Kim S, Kai Ong P, Yalcin O, Intaglietta M, Johnson PC (2009). The cell-free layer in microvascular blood flow. *Biorheology* 46(3): 181–189

- Leble V, Lima R, Dias R, Fernandes C, Ishikawa T, Imai Y, Yamaguchi T (2011) Asymmetry of red blood cell motions in a microchannel with a diverging and converging bifurcation. *Biomicrofluidics* 5:044120
- Lima R, Wada S, Takeda M, Tsubota K, Yamaguchi T (2007) In vitro confocal micro-PIV measurements of blood flow in a square microchannel: the effect of the hematocrit on instantaneous velocity profiles. *J Biomech* 40:2752–2757
- Lima R, Ishikawa T, Imai Y, Takeda M, Wada S, Yamaguchi T (2008) Radial dispersion of red blood cells in blood flowing through glass capillaries: role of hematocrit and geometry. *J Biomech* 44:2188–2196
- Lima R, Ishikawa T, Imai Y, Takeda M, Wada S, Yamaguchi T (2009a) Measurement of individual red blood cell motions under high hematocrit conditions using a confocal micro-PTV system. *Ann Biomed Eng* 37:1546–1559
- Lima R, Oliveira MSN, Ishikawa T, Kaji H, Tanaka S, Nishizawa M, Yamaguchi T (2009b) Axisymmetric polydimethylsiloxane microchannels for in vitro hemodynamic studies. *Biofabrication* 1:1–7
- Lima R, Fernandes C, Dias R, Ishikawa T, Imai Y, Yamaguchi T (2011). Microscale flow dynamics of red blood cells in microchannels: an experimental and numerical analysis. In: Tavares J (ed) *Computational vision and medical image processing: recent trends*, vol 19. Springer 297–309
- Lima R, Ishikawa T, Imai Y, Yamaguchi T (2012a). Blood flow behavior in microchannels: advances and future trends. In: Ricardo D.M, Rui L, Antonio A, Teresa M.M (eds) *Single and two-phase flows on chemical and biomedical engineering*. Bentham Sci 513–547
- Lima R, Ishikawa T, Imai Y, Yamaguchi T (2012b). Confocal micro-PIV/PTV measurements of the blood flow in micro-channels. In: Collins M.W, Koening C.S (eds), *Nano and micro flow systems for bioanalysis*. Springer, New York, 131–152
- Maeda N (1996) Erythrocyte rheology in microcirculation. *Jpn J Physiol* 46:1–14
- Maeda N, Suzuki Y, Tanaka J, Tateishi N (1996) Erythrocyte flow and elasticity of microvessels evaluated by marginal cell-free layer and flow resistance. *Am J Physiol* 271 Heart Circ Physiol 40:H2454–H2461
- MatLab (2010). The mathworks, Inc., version 7.11. Image processing toolbox version 7.1 user's guide
- Meijering E, Smal I, Danuser G (2006) Tracking in molecular bioimaging. *IEEE Signal Process Mag* 23:46–53
- Namgung B, Ong PK, Wong YH, Lim D, Chun KC, Kim S (2010) A comparative study of histogram-based thresholding of cell-free layer width in small blood vessels. *Physiol Meas* 31:N61–N70
- Pinho D, Lima R, Pereira AI, Gayubo F (2012) Automatic tracking of labeled red blood cells in microchannels. *Int J for Numer Methods Biomed Eng*. doi:[10.1002/cnm.2526](https://doi.org/10.1002/cnm.2526)
- Pinho D, Lima R, Pereira AI, Gayubo F (2013). Tracking red blood cells in microchannels: a comparative study between an automatic and a manual method. In Tavares JMRS, Natal Jorge RM (eds), *Topics in medical image processing and computational vision*, vol 8. Springer, Heidelberg. doi [10.1007/978-94-007-0726-9\\_9](https://doi.org/10.1007/978-94-007-0726-9_9)
- Pries AR, Neuhaus D, Gaehtgens P (1992) Blood viscosity in tube flow-dependence on diameter and hematocrit. *Am J Physiol* 263:H1770–H1778
- Shevkopylas SS, Yoshida T, Munn LL, Bitensky MW (2005) Biomimetic autoseparation of leukocytes from whole blood in a microfluidic device. *Anal Chem* 77:933–937
- Sollier E, Cubizolles M, Fouillet Y, Achard JL (2010) Fast and continuous plasma extraction from whole human blood based on expanding cell-free layer devices. *Biomed Microdevices* 12:485–497
- Suzuki Y, Tateishi N, Soutan M, Maeda N (1996) Deformation of erythrocytes in microvessels and glass capillaries: effects of erythrocyte deformability. *Microcirculation* 3:49–57
- Tateishi N, Suzuki Y, Soutani M, Maeda N (1994) Flow dynamics of erythrocytes in microvessels of isolated rabbit mesentery: cell-free layer and flow resistance. *J Biomech* 27:1119–1125

- Yaginuma T, Oliveira MSN, Lima R, Ishikawa T, Yamaguchi T (2011). Red blood cell deformation in flows through a PDMS hyperbolic microchannel. In: Proceedings of TechConnect World 2011—Microtech Conference and Expo, vol 2. Boston, USA, p 505
- Yaginuma T, Oliveira MSN, Lima R, Ishikawa T, Yamaguchi T (2013). Human red blood cell behavior under homogeneous extensional flow in a hyperbolic-shaped microchannel. *Biomicrofluidics* 7:054110